Cell Reports, Volume *43*

Supplemental information

Crimean-Congo hemorrhagic fever survivors elicit protective non-neutralizing antibodies that target 11 overlapping regions on glycoprotein GP38

Olivia S. Shin, Stephanie R. Monticelli, Christy K. Hjorth, Vladlena Hornet, Michael Doyle, Dafna Abelson, Ana I. Kuehne, Albert Wang, Russell R. Bakken, Akaash K. Mishra, Marissa Middlecamp, Elizabeth Champney, Lauran Stuart, Daniel P. Maurer, Jiannan Li, Jacob Berrigan, Jennifer Barajas, Stephen Balinandi, Julius J. Lutwama, Leslie Lobel, Larry Zeitlin, Laura M. Walker, John M. Dye, Kartik Chandran, Andrew S. Herbert, Noel T. Pauli, and Jason S. McLellan

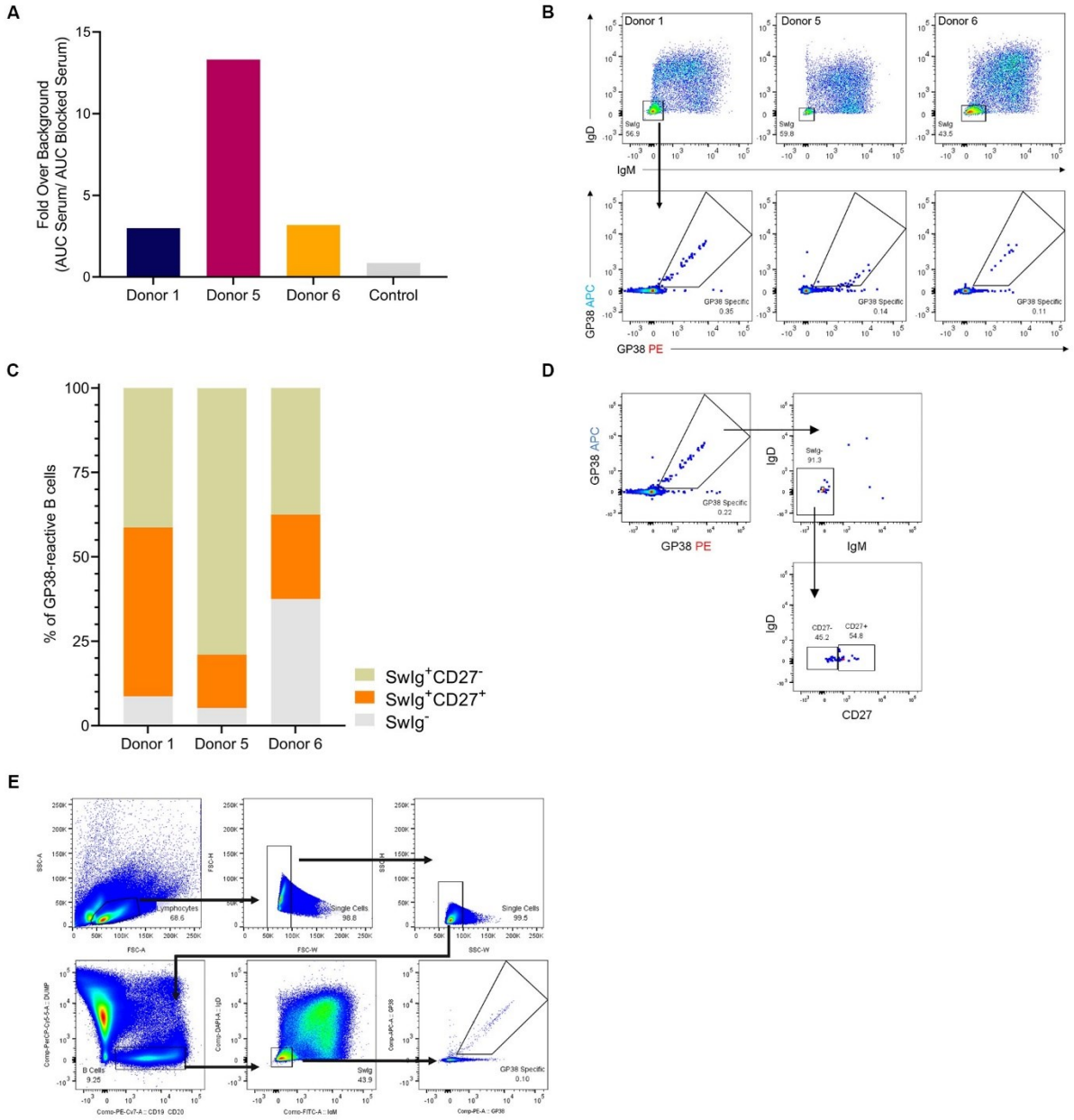

Figure S1. Serum analysis and flow cytometry, Related to Figure 1. (A) ELISA data from donor and control serum, reported as fold-over-background of area under the curve (AUC) of the serum/blocked serum. (B) Flow cytometric analysis of IgM and IgD surface expression of donor B cells (top) and avid-rGP38 binding of SwIg B cells (bottom). Donor 1 PBMCs were gated on $CD3^{-}CD8^{-}CD14^{-}CD16^{-}PI^{-}CD19^{+}$ lymphocytes; Donors 5 and 6 PMBCs were gated on $CD3^{-}CD8^{-}CD14^{-}CD16^{-}PI^{-}CD19^{+}CD20^{+}$ lymphocytes. (C) Bar chart of CD27 surface expression on rGP38-reactive SwIg B cells broken down by donor. (D) Representative gating strategy used for the calculations in panel C. Upstream of the first flow plot, PBMCs were gated on $CD3^{-}CD8^{-}CD14^{-}CD16^{-}PI^{-}CD19^{+}$ lymphocytes. (E) Example of gating strategy used to sort rGP38-reactive, SwIg B cells.

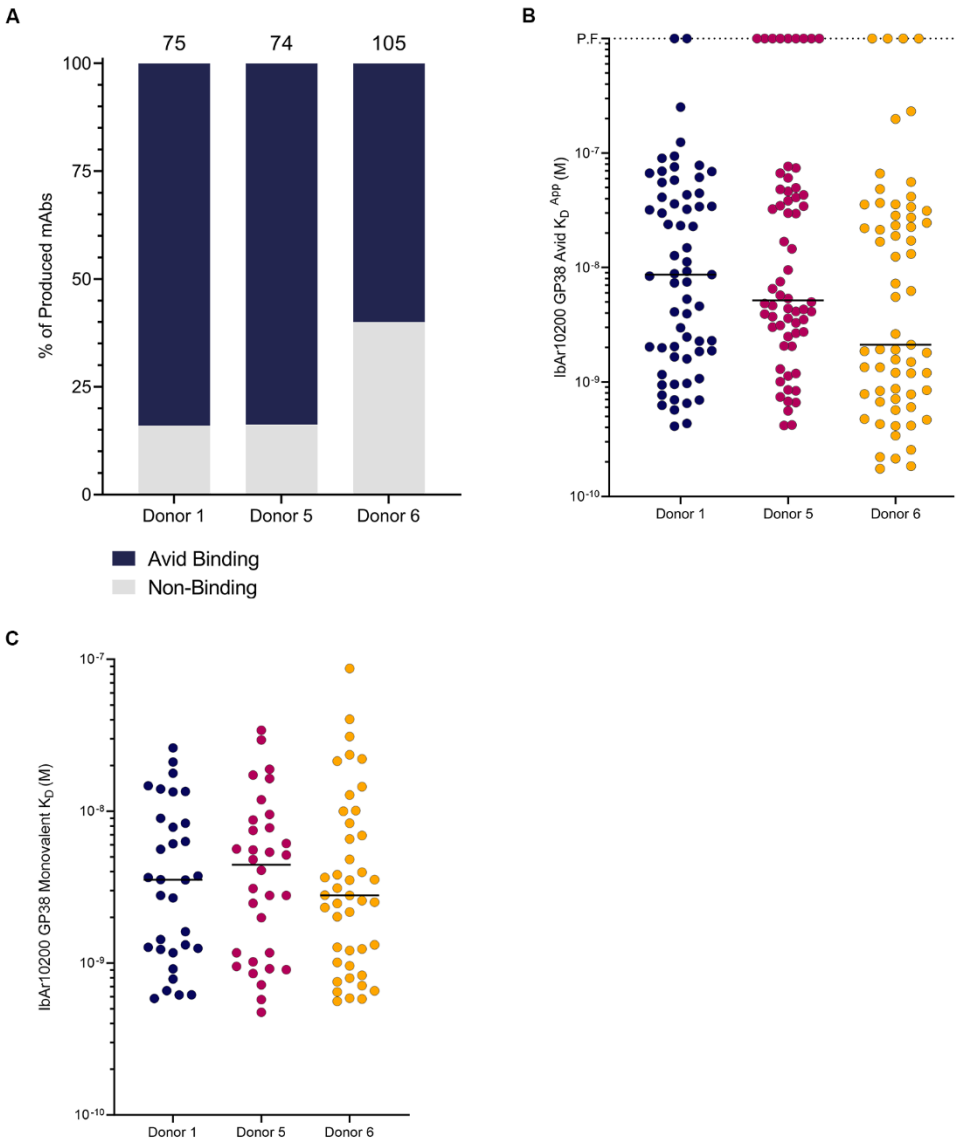

Figure S2. Avid binding analysis of antibodies from the three donors, Related to Figure 1. (A) Avid binding of the produced mAbs to IbAr10200 rGP38 protein. Total number of mAbs from each donor are indicated above each representative bar. (B) Avid $K_D$apparent (K_D^{App}) of the mAbs that bound avidly to IbAr10200 rGP38 in the assay shown in panel A. P.F. indicates poor fit of the BLI curve. (C) Single concentration monovalent K_D of the mAbs that bound monovalently to IbAR10200 rGP38 shown in **Figure 1B** with poor fitting samples removed for analysis. Black horizontal line defines median.

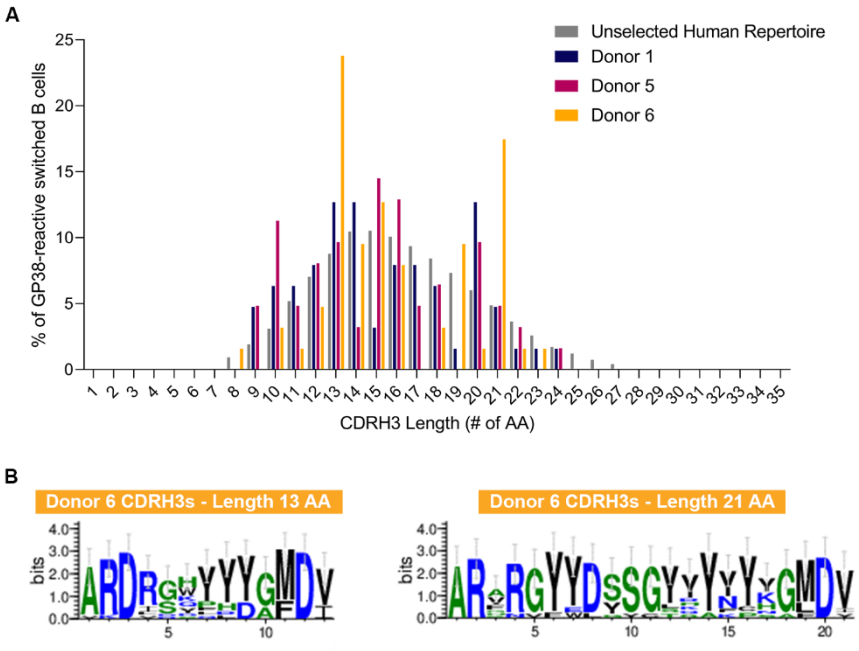

Figure S3. CDRH3 properties of isolated B cells, Related to Figure 1. (A) Analysis of CDRH3 lengths of mAbs from the three donors. (B) Logo plot representing CDRH3 sequences of mAbs cloned from Donor 6 B cells that have a length of 13 and 21 amino acids (AA), respectively. Hydrophilic amino acids (R, K, D, E, N, Q) are colored in blue; neutral amino acids (S, G, H, T, A, P) are colored in green; hydrophobic amino acids (Y, V, M, C, L, F, I, W) are colored in black. Logo plots were created using WebLogo software v3.5.0.

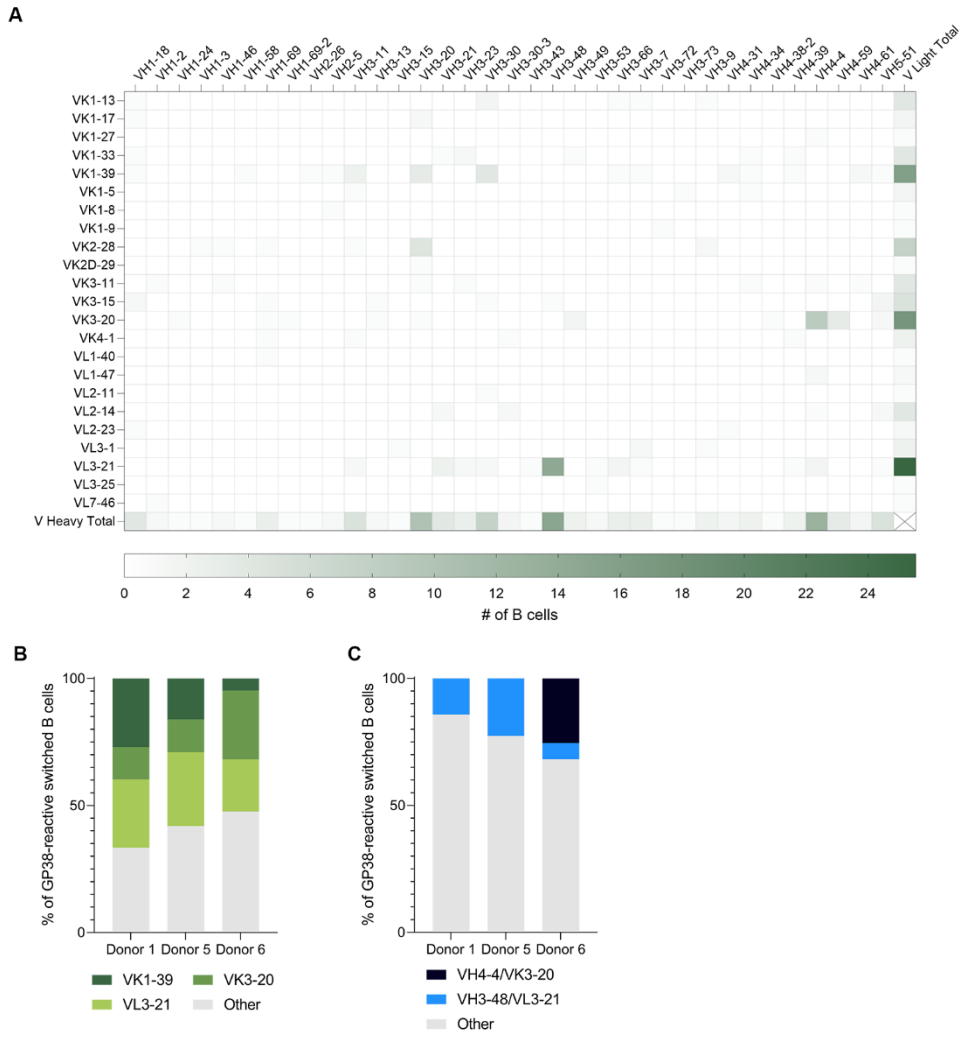

Figure S4. Germline gene usage of the B cell repertoire, Related to Figure 1. (A) Heatmap of VH and VL germline gene usage across mAbs from the three donors; shades of green represent the number of B cells that used a certain germline gene pairing. (B) Analysis of VK1-29, VK3-20, and VL3-21 germline gene usage by donor. (C) Analysis of VH4-4/VK3-20 and VH3-48/VL3-21 germline gene usage by donor.

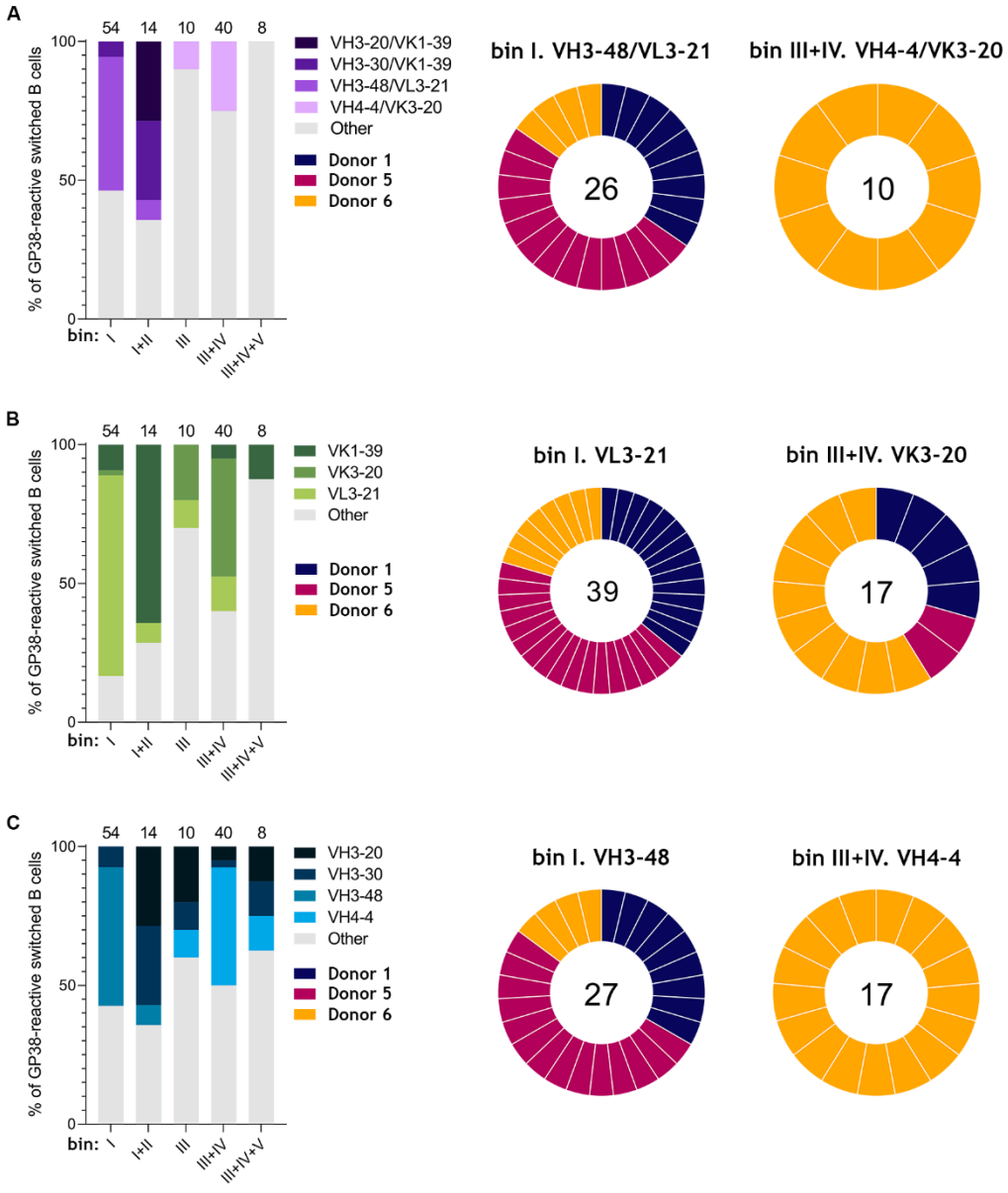

Figure S5. Germline gene usage per bin, Related to Figure 1. (A) Germline gene pairing usage per bin (left); bin I VH3-48/VL3-21 and bin III+IV VH4-4/VK3-20 germline gene usage per donor (middle and right). (B) Variable light chain germline gene usage per bin (left); bin I VL3-21 and bin III+IV VK3-20 germline gene usage per donor (middle and right). (C) Variable heavy chain germline gene usage per bin (left); bin I VH3-48 and bin III+IV VH4-4 germline gene usage per donor (middle and right). For all panels, the total number of mAbs per germline gene usage is indicated within each circular diagram.

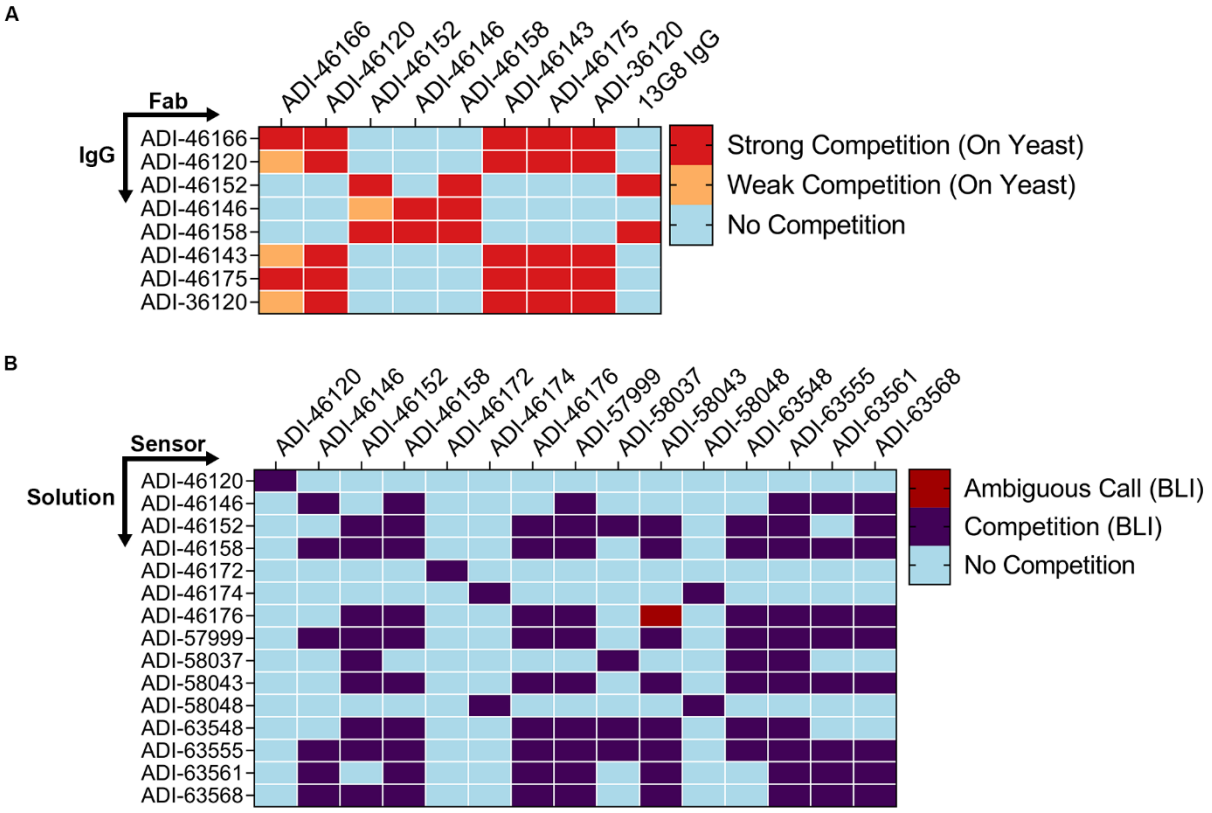

Figure S6. Preliminary cross-binning experiments, Related to Figure 2. (A) Matrix of first preliminary cross-binning experiment. Results are displayed with surface-presented IgGs on the y-axis and competitive pre-complexed Fabs on the x-axis, unless otherwise noted. (B) Matrix of second preliminary cross-binning experiment. Results were run in an IgG vs. IgG format.

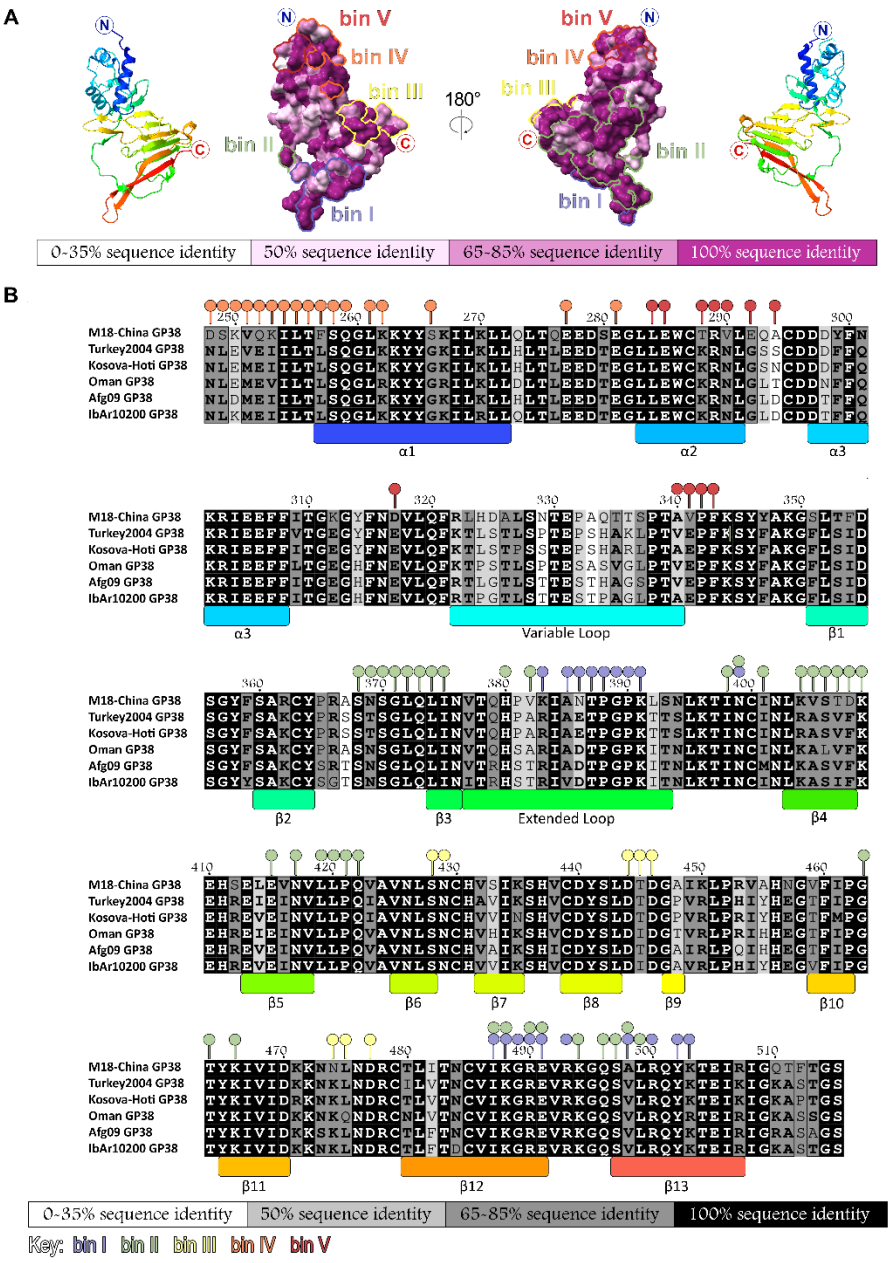

Figure S7. Conservation of CCHFV GP38 and interactions of GP38-specific antibodies, Related to Figures 3, 5, and 6. Regions of interactions for GP38-specific antibodies as identified from yeast surface display-based mapping (YSD residues that disrupted antibody binding by >75%) and high-resolution antibody structures (c13G8, ADI-46152, ADI-58048, ADI-46143) are displayed within the five main antigenic sites in corresponding colors for each bin: bin I (blue), bin II (green), bin III (yellow), bin IV (orange), and bin V (red). (A) Surface representation of IbAr10200 GP38 by sequence identity for the six isolates using ChimeraX Color by Conservation: most variable residues (white) to most conserved residues (purple). (B) Sequence alignment generated by ClustalOmega for 79121M18 (UniProt: D4NYK3), 200406546-Turkey (UniProt:

A0A0U2SQZ0), Kosova-Hoti (UniProt: B2BSL7), Oman-199809166 (UniProt: A0A0U3C6Q7), Afg09-2990 (UniProt: E5FEZ4), and IbAr10200 (UniProt: Q8JSZ3). Percent sequence identity indicated by box color: white (0-35%), light gray (50%), dark gray (65-85%), and black (100%). Sequence consensus or strong conservation among sequences is indicated by bold lettering. Secondary structure assigned for IbAr10200 GP38 from ESPript server with colored boxes from N-terminal (blue) to C-terminal (red).

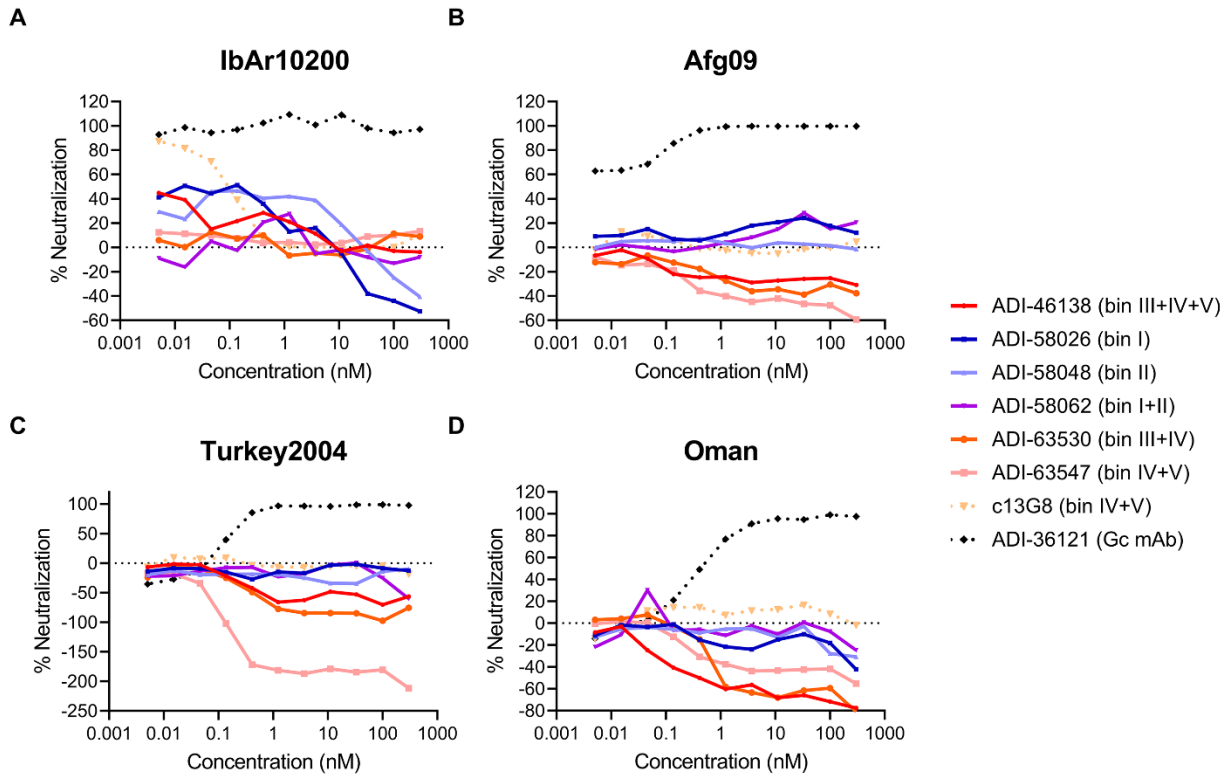

Figure S8. Authentic virus neutralization assay of GP38 mAb panel, Related to Figure 4. (A–D) Neutralization curves of the indicated mAbs against authentic (A) CCHFV IbAr10200, (B) CCHFV Afg09, (C) CCHFV Turkey2004, and (D) CCHFV Oman. Neutralization assays were conducted in VeroE6 cells. The average of n=3 each from two independent experiments (n=6 total) is shown for all neutralization curves.

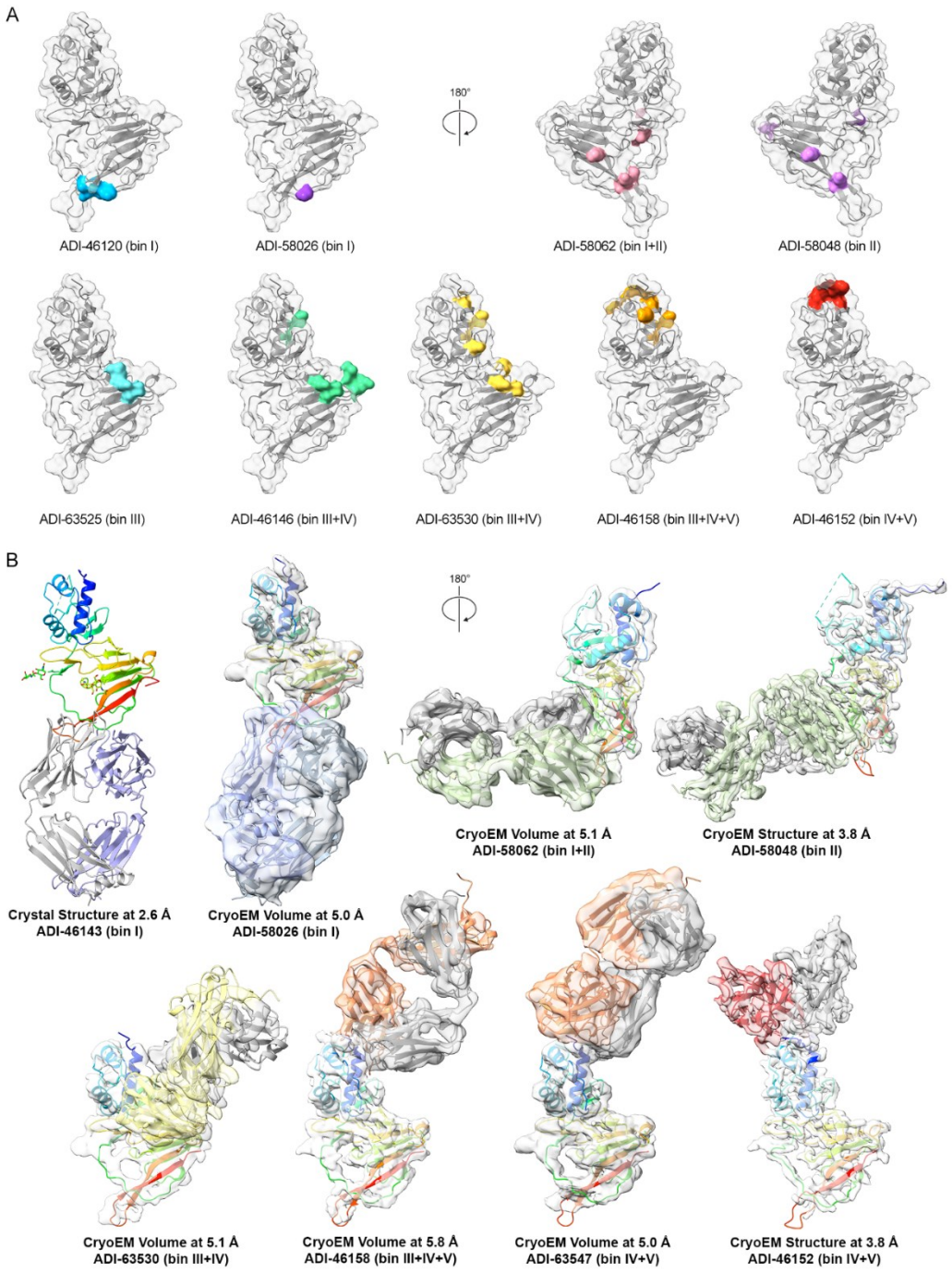

Figure S9. Structures and identified critical residues on GP38 required for antibody binding mapped across the surface of GP38, Related to Figure 5. (A) Yeast-based critical-residue mapping strategy revealed one to nine critical residues necessary for an antibody to bind to GP38. YSD residues are colored on the surface representation of CCHFV IbAr10200 GP38 (white surface). (B) GP38 bound ADI-46143 Fab crystal structure shown as ribbons. For the high-resolution cryo-EM structure of GP38+ADI-46152+ADI-58048, the refined model is docked into the cryo-EM map and displayed by each Fab. For the remaining medium-resolution cryo-EM structures, CCHFV IbAr10200 GP38 (PDB ID: 6VKF) and AlphaFold2 models are docked into

the corresponding cryo-EM maps and displayed by each Fab. Full cryo-EM complexes (GP38 bound by both Fabs) are displayed in **Figures S10**, **S11**, **S12**, and **S13**.

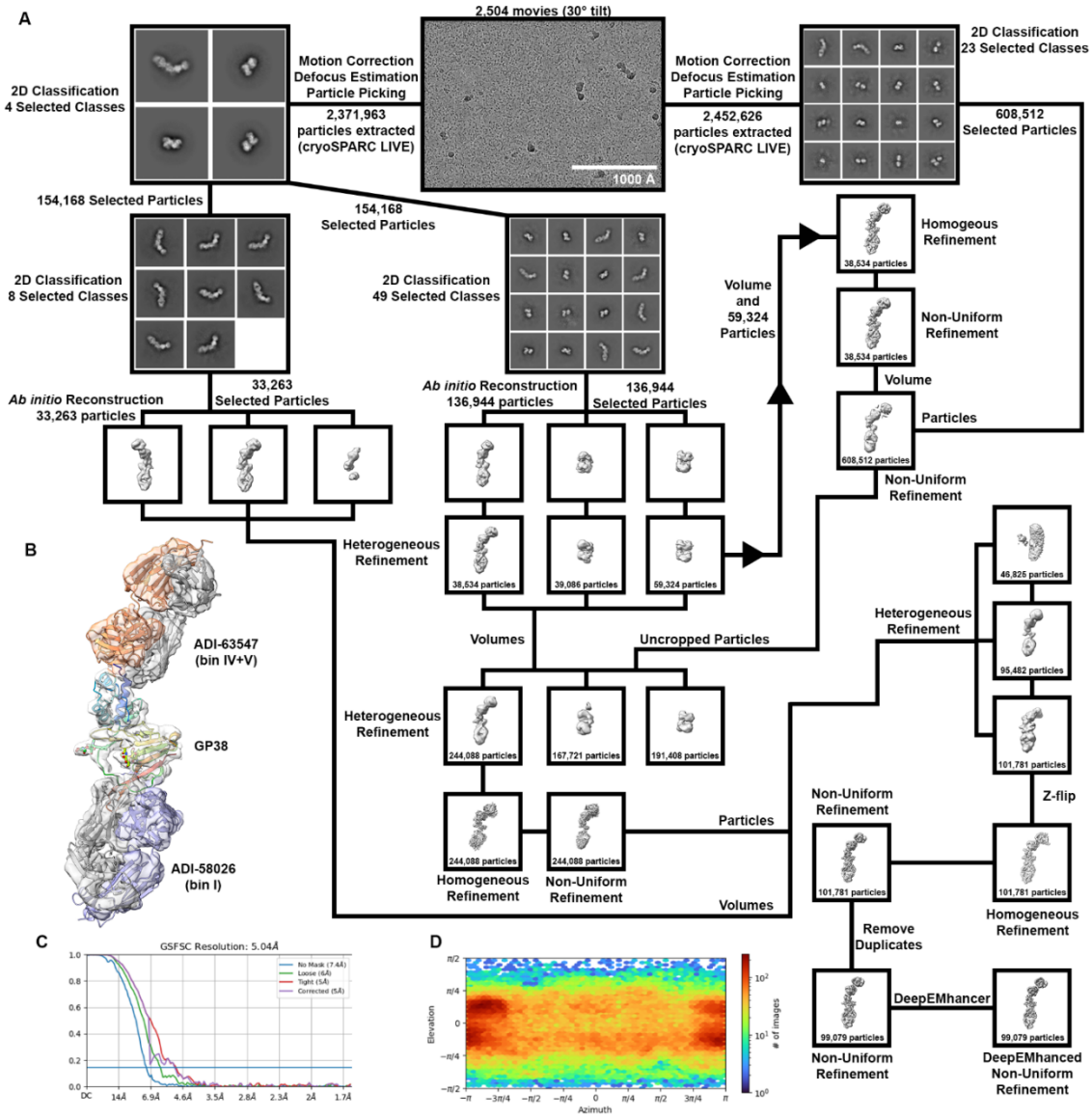

Figure S10. Structural characterization of ADI-58026 and ADI-63547 Fabs bound to CCHFV IbAr10200 GP38, Related to Figure 5. (A) Data processing and refinement pipeline for the complex. Unless otherwise noted, processing was done using cryoSPARC v3.2 and subsequent versions. (B) Cryo-EM volume of the complex with docked models of GP38 (PDB ID: 6VKF, rainbow) with ADI-58026 Fab (AlphaFold2 model, heavy chain in blue and light chain in dark gray) and ADI-63547 (AlphaFold2 model, heavy chain in orange and light chain in dark gray). (C) Gold standard FSC curve. (D) Viewing distribution plot.

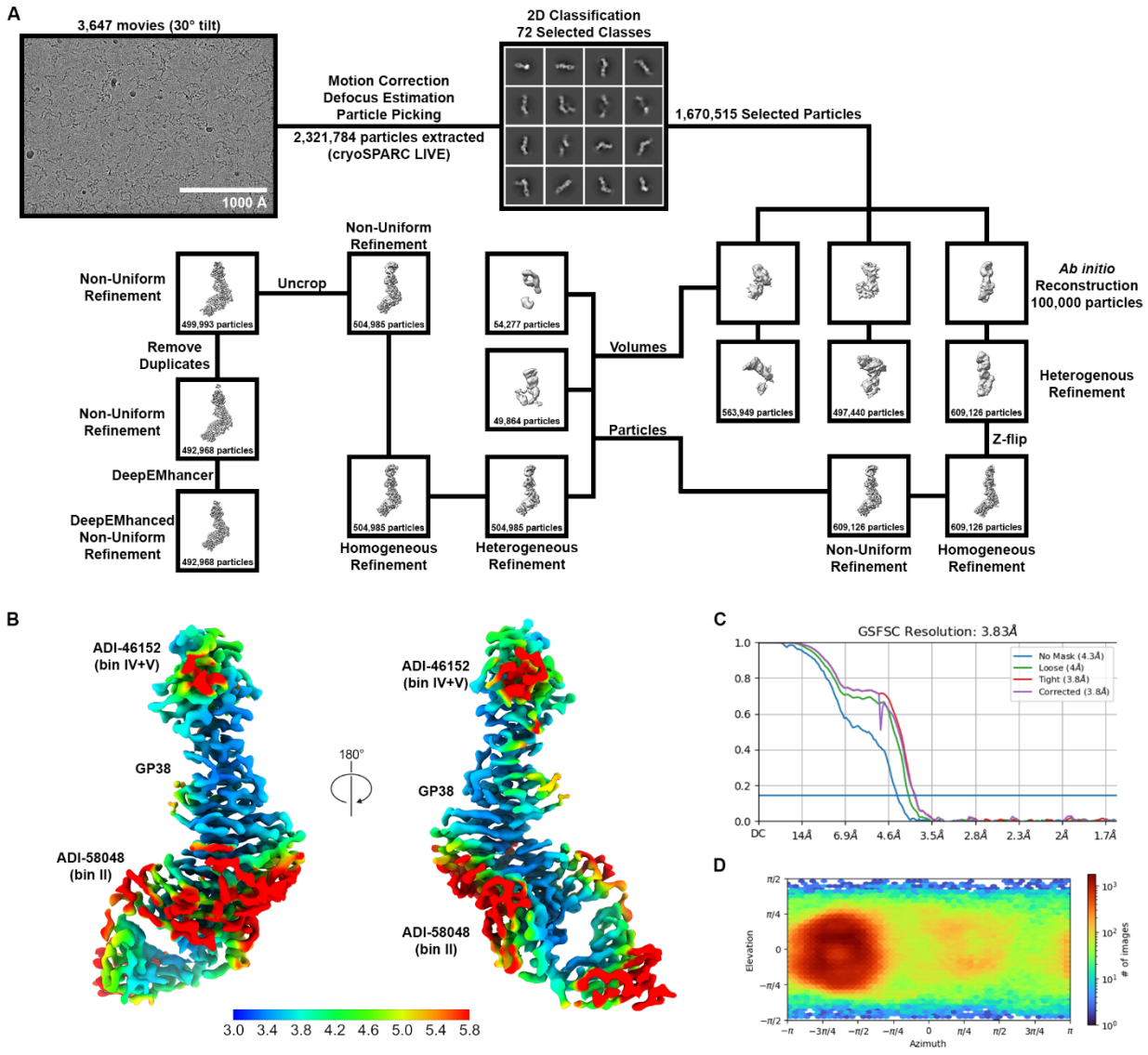

Figure S11. Structural characterization of ADI-46152 and ADI-58048 Fabs bound to CCHFV IbAr10200 GP38, Related to Figures 5 and 6. (A) Data processing and refinement pipeline for the complex. Unless otherwise noted, processing was performed using cryoSPARC v3.2 and subsequent versions. (B) Local resolution estimation of the cryo-EM structure colored as a rainbow from blue (3.0 Å) to red (5.8 Å). (C) Gold standard FSC curve. (D) Viewing distribution plot.

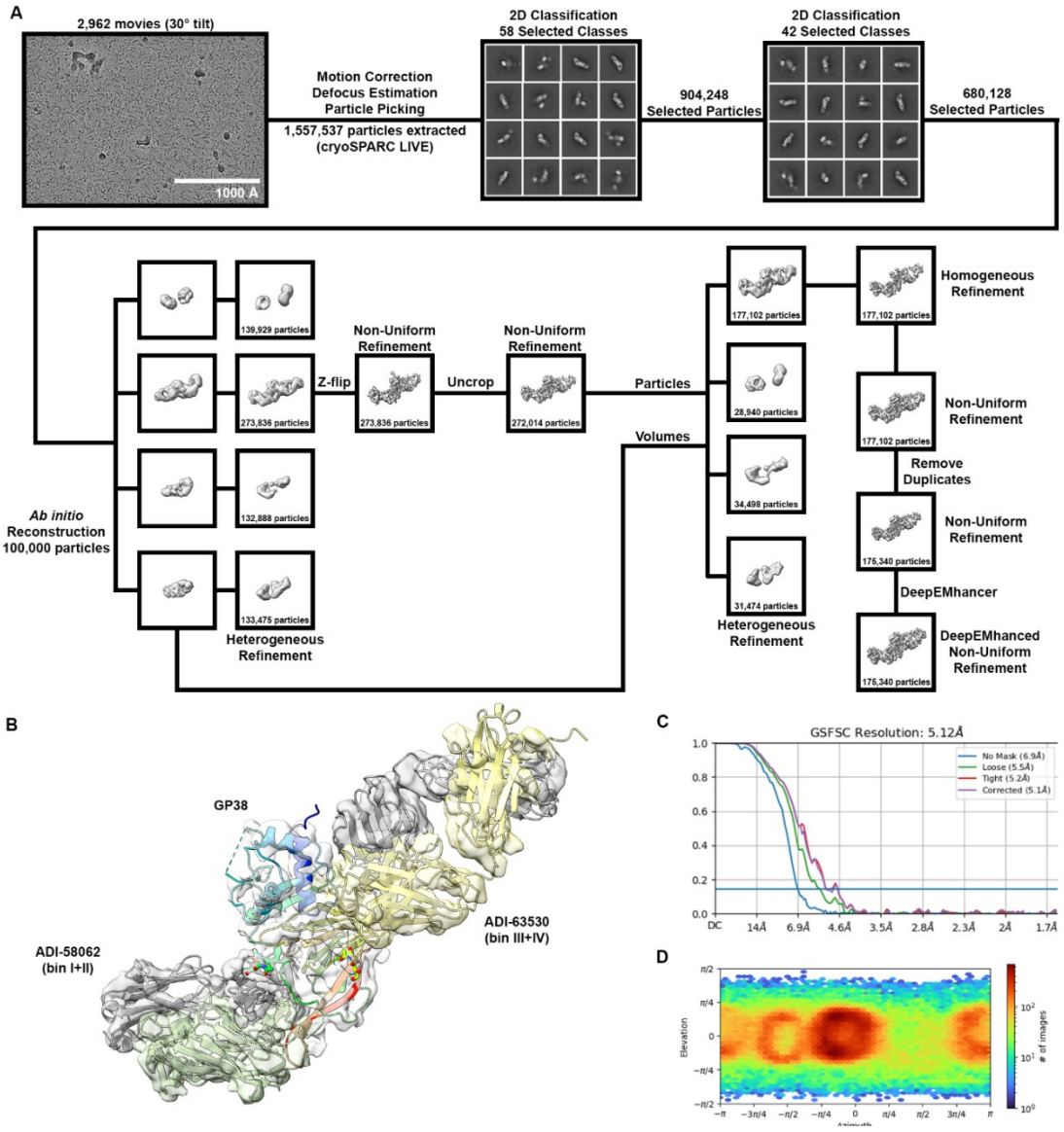

Figure S12. Structural characterization of ADI-58062 and ADI-63530 Fabs bound to CCHFV IbAr10200 GP38, Related to Figure 5. (A) Data processing and refinement pipeline for the complex. Unless otherwise noted, processing was done using cryoSPARC v3.2 and subsequent versions. (B) Cryo-EM volume of the complex with docked models of GP38 (PDB ID: 6VKF, rainbow) with ADI-58062 Fab (AlphaFold2 model, heavy chain in green and light chain in dark gray) and ADI-63530 (AlphaFold2 model, heavy chain in yellow and light chain in dark gray). (C) Gold standard FSC curve. (D) Viewing distribution plot.

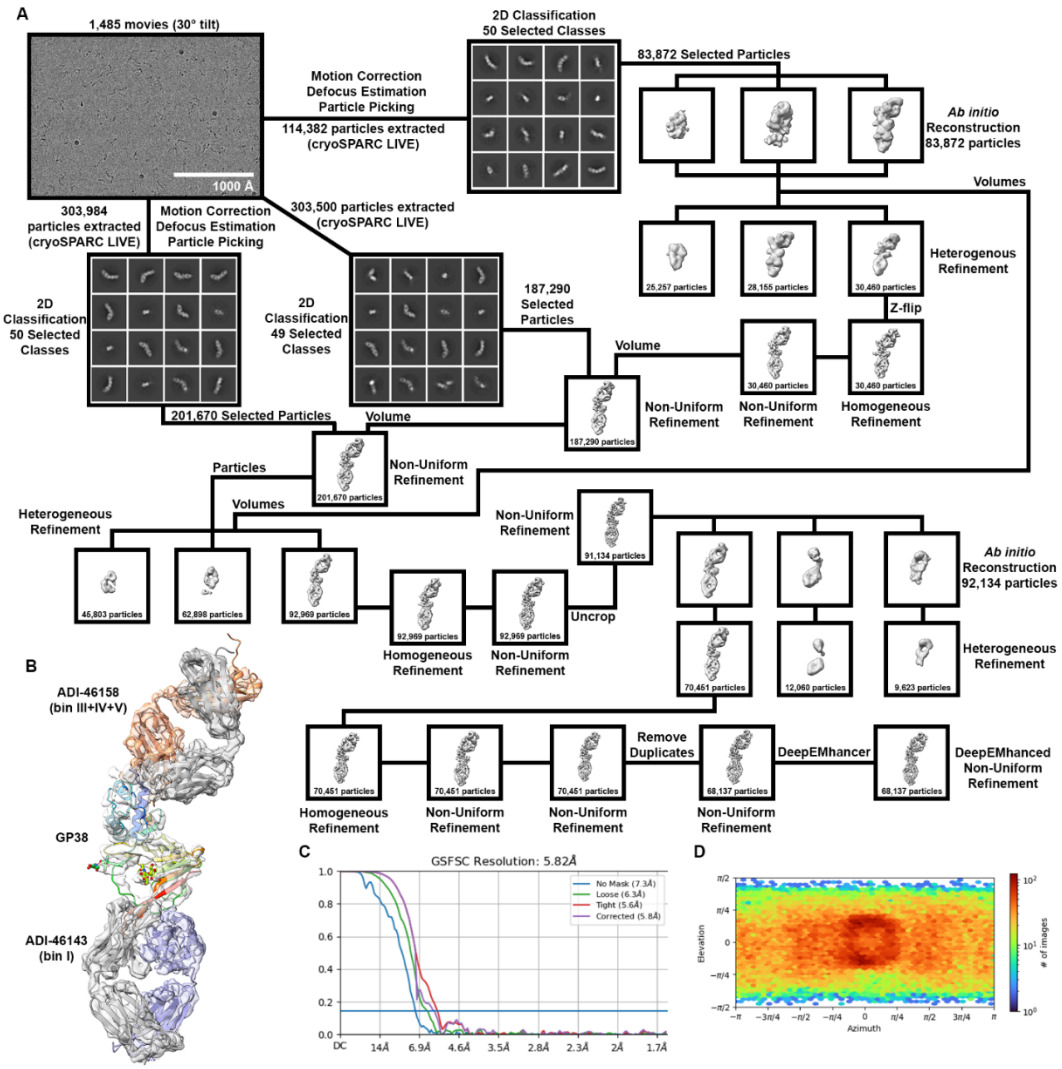

Figure S13. Structural characterization of ADI-46143 and ADI-46158 Fabs bound to CCHFV IbAr10200 GP38, Related to Figure 5. (A) Data processing and refinement pipeline for the complex. Unless otherwise noted, processing was done using cryoSPARC v3.2 and subsequent versions. (B) Cryo-EM volume of the complex with docked models of GP38 (PDB ID: 6VKF, rainbow) with ADI-46143 Fab (crystal structure, heavy chain in blue and light chain in dark gray) and ADI-46158 (AlphaFold2 model, heavy chain in orange and light chain in dark gray). (C) Gold standard FSC curve. (D) Viewing distribution plot.

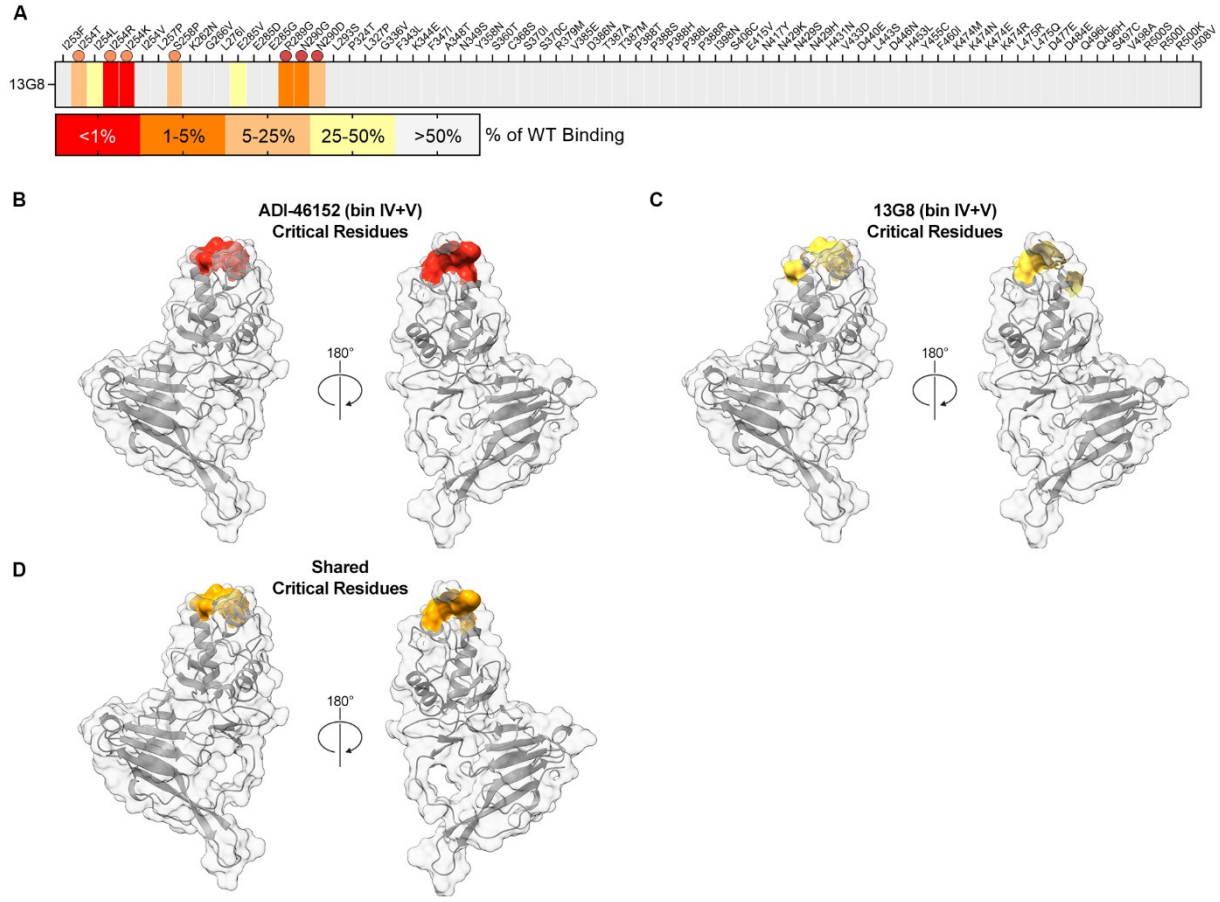

Figure S14. Identified critical residues for 13G8 binding to GP38, Related to Figure 6. (A) Yeast-based critical-residue mapping strategy for 13G8. Total loss of binding with an identified residue (red), disruption of binding (orange to yellow), and majority of binding retained (gray). Orange dots indicate bin IV critical residues and red dots indicate bin V critical residues. For panels B to D, the grouped identified critical residues on GP38 required for antibody binding overlaid onto the surface representation of GP38 for (B) ADI-46152 in red, (C) 13G8 in yellow, and (D) shared critical residues between ADI-46152 and 13G8 in orange.

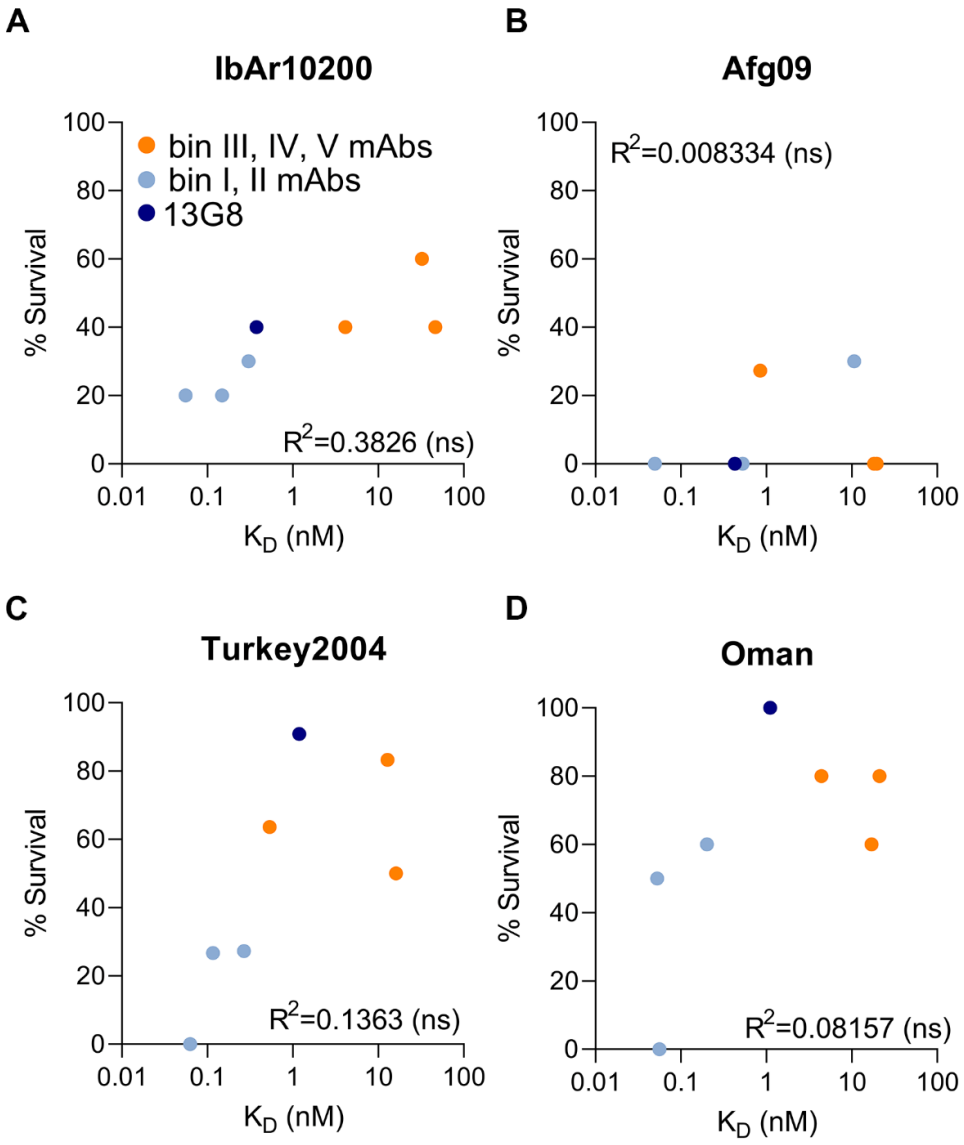

Figure S15. Correlation of K_D and protective efficacy for GP38 mAbs, Related to Figure 7. Percent survival of mice from experiments in **Figure 7** are plotted versus K_D determinations from SPR experiments in **Figure 3C** for each respective isolate (A, IbAr10200; B, Afg09-2990; C, Turkey2004; D, Oman). mAbs that are bin III and/or IV and/or V competitors are colored orange and mAbs that are bin I and/or II competitors are colored light blue. 13G8 is colored navy. R-squared calculated by Spearman's correlation coefficient. ns is non-significant.

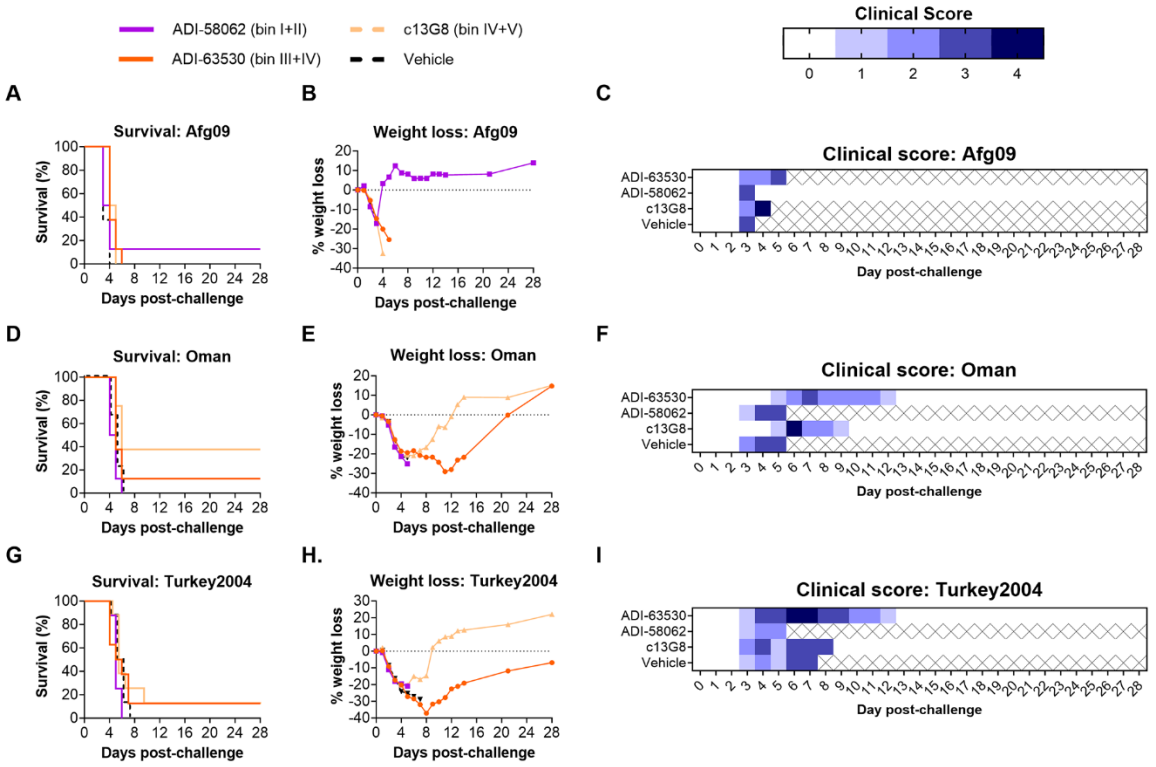

Figure S16. Cross-clade therapeutic efficacy of lead GP38 mAbs, Related to Figure 7. STAT1$^{-/-}$ mice were challenged with (A–C) CCHFV-Afg09, (D–F) CCHFV-Oman, or (G–I) CCHFV-Turkey2004 and then treated with 1 mg/mouse of mAb or vehicle 1- and 4-days post-challenge (2 mg total; n=8 mice per group). (A, D, G) Survival curves. (B, E, H) Associated mean weight loss. (C, F, I) Clinical scores are defined as: 1 = decreased grooming and/or ruffled fur, 2 = subdued behavior when un-stimulated, 3 = lethargy, hunched posture, and/or subdued behavior even when stimulated, 4 = bleeding, unresponsiveness, severe weakness, or inability to walk. Mice scoring a 4 were considered moribund and were humanely euthanized based on IACUC-approved criteria (denoted as X over white).

Donor ID	Sex	Birth Year	Date of Infection	Date of Blood Donation	Time Post-Infection (months)	Diagnostic Method	Hospitalization Time (days)	District
1	Male	1949	Aug 2013	Jun 2017	46	PCR	14	Agago
5	Male	1982	Nov 2015	Nov 2017	24	PCR	14	Nakaseke
6	Male	1987	Aug 2017	Nov 2017	3	PCR	>28	Nakaseke

Table S1. Patient metadata of CCHFV-convalescent donors, Related to Figure 1. Date of infection, blood donation, and hospitalization time are approximate.

Bin Code	Competing Antibodies
I	**ADI-46120**
I + II	ADI-46120 & ADI-58048
I + III	ADI-46120 & ADI-46146
I + IV	ADI-46120 & ADI-46158
II	**ADI-58048**
III	**ADI-46146**
III + IV	ADI-46146 & ADI-46158
III + IV + V	ADI-46146 & ADI-46158 & ADI-46152
IV	**ADI-46158**
IV + V	ADI-46158 & ADI-46152
V	**ADI-46152**
Unknown/Weak Affinity	NA

Table S2. Bin code and representative antibody table, Related to Figure 2. Antibodies representative of each of the discrete antigenic sites (bold font) along with the overlapping bins (non-bold font).

Clone	Donor	Bin Code	V Heavy	V Light
ADI-58026	Donor 1	I	VH3-66	VL3-21
ADI-58062	Donor 1	I+II	VH3-20	VK1-39
ADI-58048	Donor 1	II	VH4-39	VK1-39
ADI-63530	Donor 6	III+IV	VH3-21	VL3-21
ADI-46138	Donor 5	III+IV+V	VH1-69	VK2-28
ADI-63547	Donor 6	IV+V	VH1-69	VK4-1

Table S3. Germline gene usage of mAbs used in further characterization and protection studies, Related to Figure 3. Variable heavy chain and variable light chain gene information for mAbs selected for subsequent studies.

Clone	PSR Score (0-1)	HIC Retention Time (min)	Fab T_m by DSF (°C)
ADI-46138	0	9.7	73
ADI-58026	0	9.4	67
ADI-58048	0.09	11.5	79
ADI-58062	0	9.8	67
ADI-63530	0.05	9.2	63.5
ADI-63547	0.1	10.9	75

Clean PSR: < 0.10	Clean to Low HIC: < 10.5 min	Tm > 65.0 °C
Low PSR: ≥ 0.10 and < 0.33	Medium HIC: ≥ 10.5 and < 11.5 min	Tm < 65.0 °C
Medium PSR: ≥ 0.33 and < 0.66	High HIC: ≥ 11.5 min	
High PSR: ≥ 0.66 and ≤ 1.00		

Table S4. Developability metrics for the six mAbs used in protection studies, Related to Figure 3. Table describing the developability properties of lead mAbs[1]. Poly-Specificity Reagent (PSR) indicates relative level of poly-specificity in each mAb normalized against standard control IgGs. Hydrophobicity Interaction Chromatography (HIC) measures mAb interaction with a HIC column as a normalized time to elution off the column. Fab Tm provides a measure of antibody thermostability using differential scanning fluorimetry (DSF) and is reported as the lowest temperature event distinct from a constant-heavy-2 (CH2) signal.

		ADI-58026 (bin I)	ADI-58062 (bin I+II)	ADI-58048 (bin II)	ADI-63530 (bin III+IV)	ADI-46138 (bin III+IV+V)	ADI-63547 (bin IV+V)	13G8 (bin IV+V)
IbAr10200 GP38	K_D (M)	<5.58E-11	1.48E-10	<3.04E-10	3.24E-08	4.12E-09	4.67E-08	3.76E-10
	k_a (1/Ms)	3.06E+06	3.24E+06	5.62E+05	2.32E+05	1.53E+06	1.92E+05	8.58E+05
	k_d (1/s)	<1.71E-4	4.80E-04	<1.71E-4	7.50E-03	6.30E-03	8.98E-03	3.22E-04
	Rmax	126.1	93.8	97.4	68.4	88.4	123.0	204.4
Oman GP38	K_D (M)	<5.25E-11	<5.59E-11	<2.02E-10	1.70E-08	4.40E-09	2.11E-08	1.11E-09
	k_a (1/Ms)	3.26E+06	3.06E+06	8.48E+05	3.62E+05	1.33E+06	3.22E+05	1.02E+06
	k_d (1/s)	<1.71E-4	<1.71E-4	<1.71E-4	6.15E-03	5.86E-03	6.78E-03	1.13E-03
	Rmax	114.0	86.1	144.3	82.0	92.0	113.2	181.8
Kosova-Hoti GP38	K_D (M)	1.16E-10	7.86E-11	<2.66E-10	1.50E-08	5.68E-10	1.83E-08	6.00E-10
	k_a (1/Ms)	2.22E+06	2.92E+06	6.43E+05	3.31E+05	1.30E+06	2.88E+05	1.06E+06
	k_d (1/s)	2.56E-04	2.30E-04	<1.71E-4	4.97E-03	7.40E-04	5.26E-03	6.34E-04
	Rmax	117.6	103.3	150.6	78.7	86.8	116.3	183.4
Turkey2004 GP38	K_D (M)	1.16E-10	<6.27E-11	<2.68E-10	1.28E-08	5.35E-10	1.62E-08	1.19E-09
	k_a (1/Ms)	2.59E+06	2.73E+06	6.37E+05	3.05E+05	1.30E+06	2.81E+05	8.72E+05
	k_d (1/s)	3.01E-04	<1.71E-4	<1.71E-4	3.91E-03	6.95E-04	4.56E-03	1.04E-03
	Rmax	118.0	108.2	121.5	77.9	124.5	115.9	184.4
Afg09 GP38	K_D (M)	<4.94E-11	5.25E-10	1.07E-08	1.82E-08	8.51E-10	1.96E-08	4.27E-10
	k_a (1/Ms)	3.46E+06	2.64E+06	2.91E+05	2.38E+05	1.30E+06	2.71E+05	1.19E+06
	k_d (1/s)	<1.71E-4	1.39E-03	3.10E-03	4.32E-03	1.10E-03	5.31E-03	5.09E-04
	Rmax	113.8	100.9	111.1	77.7	114.4	110.9	176.7
M18-China GP38	K_D (M)	<3.31E-11	<8.99E-11	<3.98E-10	1.76585E-08	4.35E-09	1.61E-08	P.F.
	k_a (1/Ms)	5.17E+06	1.90E+06	4.30E+05	2.69E+05	5.06E+05	3.22E+05	N.A.
	k_d (1/s)	<1.71E-4	<1.71E-4	<1.71E-4	4.75E-03	2.20E-03	5.20E-03	N.A.
	Rmax	109.6	104.2	113.3	77.1	127.6	106.7	N.A.

Table S5. Carterra kinetics of GP38 antibodies, Related to Figure 3. Multi-concentration Carterra kinetics data of the six mAbs used in protection studies against rGP38 protein of six tested clinical isolates. Samples for which the off-rate was limited are denoted as < the k_d and calculated K_D. The sample for which a curve could not be fit is denoted as P.F and shaded in blue.

Complex Composition	CCHFV IbAr10200 GP38 + ADI-46152 Fab + ADI-58048 Fab	CCHFV IbAr10200 GP38 + ADI-58026 Fab + ADI-63547 Fab	CCHFV IbAr10200 GP38 + ADI-58062 Fab + ADI-63530 Fab	CCHFV IbAr10200 GP38 + ADI-46143 Fab + ADI-46158 Fab
Data Collection				
EMDB	EMD-43604	EMD-43553	EMD-43552	EMD-43551
Microscope (FEI)	Titan Krios	Titan Krios	Titan Krios	Titan Krios
Voltage (kV)	300	300	300	300
Detector	Gatan K3	Gatan K3	Gatan K3	Gatan K3
Magnification	105,000X	105,000X	105,000X	105,000X
Pixel size (Å/pix)	0.8332	0.8332	0.8332	0.8332
Exposure rate (e^-/pix/sec)	8	8	8	8
Frames per exposure	100	100	100	100
Exposure (e^-/Å^2)	80	80	80	80
Defocus range (μm)	1.5-2.5	1.5-2.5	1.5-2.5	1.5-2.5
Tilt angle (degrees, °)	30	30	30	30
Micrographs collected	5,364	3,141	3,262	1,515
Micrographs used	3,647	2,504	2,962	1,485
Automation software	SerialEM	SerialEM	SerialEM	SerialEM
Particles extracted (total)	2,321,784	2,452,626	1,557,537	303,984
Final 3D Reconstruction Statistics				
PDB	8VWW	n/a	n/a	n/a
Particles	492,968	99,079	176,340	68,137
Symmetry imposed	n/a (C1)	n/a	n/a	n/a
Map sharpening *B*-factor	-173.7	-266.1	-329.5	-462.9
Resolution at FSC…				
Unmasked: 0.5 (Å)	4.1	9.9	8.6	8.1
Masked: 0.5 (Å)	4.1	9.5	8.4	7.4
Unmasked: 0.143 (Å)	3.8	5.1	5.1	5.9
Masked: 0.143 (Å)	3.8	4.9	5.1	5.6
Model Refinement and Validation Statistics				
Refinement package	Phenix	n/a	n/a	n/a
Refinement tool	Real-space refinement	n/a	n/a	n/a
Refinement Strategies	min global, local_grid_search,	n/a	n/a	n/a
Initial Models	PDB ID: 6VKF AlphaFold2 Fab	PDB ID: 6VKF AlphaFold2 Fab	PDB ID: 6VKF AlphaFold2 Fab	PDB ID: 6VKF AlphaFold2 Fab
Composition				
Amino Acids (#)	899	n/a	n/a	n/a
Ligands (Type: #)	0	n/a	n/a	n/a
Average B-factors				
Amino acids	92.3	n/a	n/a	n/a
R.m.s. deviations				
Bond lengths (Å)	0.003 (0)	n/a	n/a	n/a
Bond angles (°)	0.633 (0)	n/a	n/a	n/a
Ramachandran (%)				
Favored	95.4	n/a	n/a	n/a
Allowed	4.5	n/a	n/a	n/a

Outliers	0.1	n/a	n/a	n/a
Rotamer outliers (%)	2.05	n/a	n/a	n/a
C-β outliers (%)	0.00	n/a	n/a	n/a
CaBLAM outliers (%)	2.54	n/a	n/a	n/a
CC (mask)	0.75	n/a	n/a	n/a
MolProbity score	1.77	n/a	n/a	n/a
Clash score	4.35	n/a	n/a	n/a
EMRinger score	2.86	n/a	n/a	n/a

Table S6. Cryo-EM data collection, reconstruction, and model validation statistics, Related to Figures 5 and 6.

Complex Composition	**CCHFV IbAr10200 GP38 and ADI-46143 Fab**	**CCHFV IbAr10200 GP38 and c13G8 Fab**
PDB ID	8VVK	8VVL
Reservoir solution for crystallization	0.2 M (NH_4)-Citrate pH 7.5 9. 3% (w/v) PEG 3350 12.6% (v/v) 2-PropOH	2 M ammonium sulfate 0.1 M Bis-Tris pH 5.5 0.01 M cobalt chloride hexahydrate
Data collection		
Space group	*P* 6_1 2 2	*I* 1 2 1
Wavelength (Å)	0.979	0.979
Cell dimensions		
a, *b*, *c* (Å)	149.7, 149.7, 315.7	100.4, 67.6, 141.0
α, β, γ (°)	90, 90, 120	90, 96.5, 90
Resolution range (Å)	64.83-2.61 (2.67-2.61)	45.16-1.80 (1.84-1.80)
R_{merge}	0.027 (0.262)	0.033 (0.269)
$I/\sigma(I)$	15.6 (2.8)	9.5 (2.5)
$CC_{1/2}$	0.999 (0.814)	0.998 (0.915)
Completeness (%)	99.93 (99.86)	94.50 (92.89)
Redundancy	2.0 (2.0)	1.9 (1.9)
Total reflections	128,324 (12,566)	157,627 (15,257)
Unique reflections	64,162 (6,283)	81,877 (8,008)
Refinement		
Resolution range (Å)	59.95-2.61 (2.70-2.61)	45.16-1.80 (1.87-1.80)
Unique reflections	64,131 (6,274)	81,792 (7,990)
R_{work} / R_{free} (%)	17.71/21.71 (24.66/33.15)	19.97/21.54 (30.17/33.95)
Number of atoms	10,654	5,823
Protein	10,294	5,121
Solvent	237	623
Ligands	123	79
Average *B*-factor ($Å^2$)	59.3	41.0
Protein	59.2	40.0
Solvent	50.2	47.0
Ligands	89.4	56.5
R.m.s. deviations		
Bond lengths (Å)	0.005	0.004
Bond angles (°)	0.75	0.76
Ramachandran (%)		
Favored	96.5	98.1
Allowed	3.3	1.9
Outliers	0.2	0.0

Data in parentheses are for the highest resolution shell.

Table S7. Crystallographic data collection and refinement statistics, Related to Figures 5 and 6.

Supplemental References

1. Jain, T., Sun, T., Durand, S., Hall, A., Houston, N.R., Nett, J.H., Sharkey, B., Bobrowicz, B., Caffry, I., Yu, Y., et al. (2017). Biophysical properties of the clinical-stage antibody landscape. Proc Natl Acad Sci U S A *114*, 944-949. 10.1073/pnas.1616408114.